Electronic Supplementary Information

Experimental section

Materials: $Co(NO_3)_2 \cdot 6H_2O$, $MnSO_4 \cdot H_2O$, NH_4F, urea, KOH, and NaH_2PO_2 were purchased from Chengdu Kelong Chemical Regent Co. Ltd (China). Ni foam (NF) was purchased from Hongshan District, Wuhan Instrument Surgical Instruments business. Activated carbon (AC) was bought from Fuzhou Yihuan Carbon Co. Ltd (China). All chemicals were analytical grade and used without further purification. The water used throughout all experiments was purified through a Millipore system.

Preparation of Mn-CoP/NF and CoP/NF: Prior to synthesis, a piece of NF (2 cm×3 cm) was treated with 3 M HCl solution in an ultrasonic bath for 10 min to remove the oxide layer, and then ultrasonically washed with deionized water and ethanol for 10 min. Mn-Co-hydroxide nanowire array was prepared as follows. $MnSO_4 \cdot H_2O$ (0.2 mmol), $Co(NO_3)_2 \cdot 6H_2O$ (2 mmol), urea (10 mmol), NH_4F (5 mmol) were dissolved in 40 mL distilled water. After gentle stirring for 15 min, the pink homogenous solution and a piece of treated NF were transferred to a 50 mL Teflon-lined stainless steel autoclave. The autoclave was sealed and maintained at 120 °C for 6 h in an electric oven. After the autoclave cooled down at room temperature, the resulting MnCo precursor was taken out and washed with water and ethanol several times, followed by drying at 60 °C. To obtain Mn-CoP/NF, the resulting Mn-Co hydroxide precursor on NF and NaH_2PO_2 were put at two separate positions in a porcelain boat with 0.5 g NaH_2PO_2 at the upstream side of the furnace. After flushed with Ar, the center of the furnace was elevated to 300 °C at a ramping rate of 2 °C min^{-1} and held at this temperature for 2 h, and then naturally cooled to ambient temperature under Ar. $Mn_{0.05}$-CoP/NF, $Mn_{0.2}$-CoP/NF and CoP/NF were made by varying the atomic ratio of Mn:Co in solutions to 0.1:2, 0.4:2 and 0:2, respectively, under otherwise identical experimental conditions used for preparing Mn-CoP/NF. The mass loading were about 6.66 mg cm^{-2}. Mn-CoP on Ti mesh (Mn-CoP/TM) and Mn-CoP on carbon cloth (Mn-CoP/CC) were made by varying the substrate into Ti

mesh and CC, under otherwise identical experimental conditions used for preparing Mn-CoP/NF. The mass loading for Mn-CoP/TM and Mn-CoP/CC were about 0.96 mg cm^{-2} and 1.31 mg cm^{-2}, respectively.

Characterizations: Powder X-ray diffraction (XRD) patterns were performed using a RigakuD/MAX 2550 diffractometer with Cu Kα radiation (λ=1.5418 Å). Scanning electron microscope (SEM) measurements were recorded on a XL30 ESEM FEG scanning electron microscope at an accelerating voltage of 20 kV. The structures of the samples were determined by Transmission electron microscopy (TEM) images on a HITACHI H-8100 electron microscopy (Hitachi, Tokyo, Japan) operated at 200 kV. X-ray photoelectron spectroscopy (XPS) data of the samples was collected on an ESCALABMK II x- ray photoelectron spectrometer using Mg as the exciting source. Inductively coupled plasma mass spectrometry (ICP-MS) analysis was performed on Thermo Scientific iCAP6300.

Electrochemical measurements: The NF loaded with CoP and Mn-CoP were used as bind-free positive electrodes without further treatment. All the electrochemical measurements of samples were carried out by using a three-electrode system on a RST electrochemical workstation (Zhengz-hou Shiruisi Technology Co., Ltd.). The as-prepared samples, Hg/HgO, and Pt foil were employed as working electrode, reference electrode, and counter electrode, respectively. All the electrochemical tests include cyclic voltammetry (CV), galvanostatic charge-discharge (GCD), and electrochemical impedance spectroscopy (EIS). The CV tests were performed in the potential window of 0-0.6 V at the scan rate of 2, 5, 10, 20, 30, 40, and 50 mV s^{-1}. The GCD tests were conducted in the potential window of 0-0.5 V at the current density of 1, 2, 5, 10, 20, 30, 40, and 50 mA cm^{-2}. The EIS tests were collected using a frequency ranging from 100 kHz to 0.01 Hz. Finally, 6 M KOH was used as the electrolyte for all the electrochemical measurements.

Fabrication of asymmetric supercapacitor: The asymmetric supercapacitor (ASC) was assembled using Mn-CoP/NF (1×1 cm) as the positive electrode, AC as negative electrode, and non-woven fabrics as separator. The negative electrode was prepared

by mixing the activated carbon, acetylene black, and PVDF (which was dissolved in N-methyl pyrrolidone with a concentration of 6 mg mL^{-1}) in the mass ratio 8:1:1. The mixtures were ground adequately to form a slurry. After that, the slurry was pasted onto the treated NF (1×1 cm) and dried at 80 ℃ for 12 h.

Specific capacitance calculation: Areal capacitances (F cm^{-2}) were calculated from CV (C_{s1}) and GCD (C_{s2}) curves utilizing Formula S1[1] and Formula S2[2], respectively, where I_1 (A) is the response current, ΔV (V) is the voltage window, v (V s^{-1}) is the scan rate, I_2 (A) is the constant current, Δt (s) is the discharging time, and S (cm^2) is the geometrical area of the electrode.

$$C_{s1} = \frac{\int I_1 dV}{vS\Delta V} \qquad \text{Formula S1}$$

$$C_{s2} = \frac{I_2 \Delta t}{S\Delta V} \qquad \text{Formula S2}$$

The mass capacitances (F g^{-1}) were calculated from GCD curves utilizing Formula S3[2], where the C_m (F g^{-1}) is the mass specific capacitance, I is the response current (A), m is the mass of activate materials loaded on the Ni foam, Δt is the discharge time, ΔV is potential window of the discharge process.

$$C_m = \frac{I\Delta t}{m\Delta V} \qquad \text{Formula S3}$$

The determination for loading of AC on coated on NF: The area and mass specific capacitances of the supercapacitor device calculated from the GCD curves is analogous to those for single electrode. The mass loading of AC was determined by balancing the charges stored in each electrode. Its specific mass was calculated by the following formula,[3] Where m is the mass loading, C_{s+} and C_{m-} represent the specific capacitance of positive electrode (F cm^{-2}) and negative electrode (F g^{-1}) respectively. ΔV is the potential window of positive (+) and negative (-) electrode. S is the area of electrodes. m_- is the mass of negative electrode.

$$C_{s+} \Delta V_+ S = C_{m-} \Delta V_- m_- \qquad \text{Formula S4}$$

The calculations for energy density and power density of the ASC devices: The energy density (E) and power density (P) are obtained from the GCD curves according to the following formulas[4]: where E (Wh kg^{-1}) is the energy density, C (F g^{-}

[1]) is the mass specific capacitance, ΔV (V) is the voltage window, P (W kg^{-1}) refers to the power density and Δt (s) is the discharge time.

$$E = \frac{1}{2} C \Delta V^2 \qquad \text{Formula S5}$$

$$P = \frac{E}{\Delta t} \qquad \text{Formula S6}$$

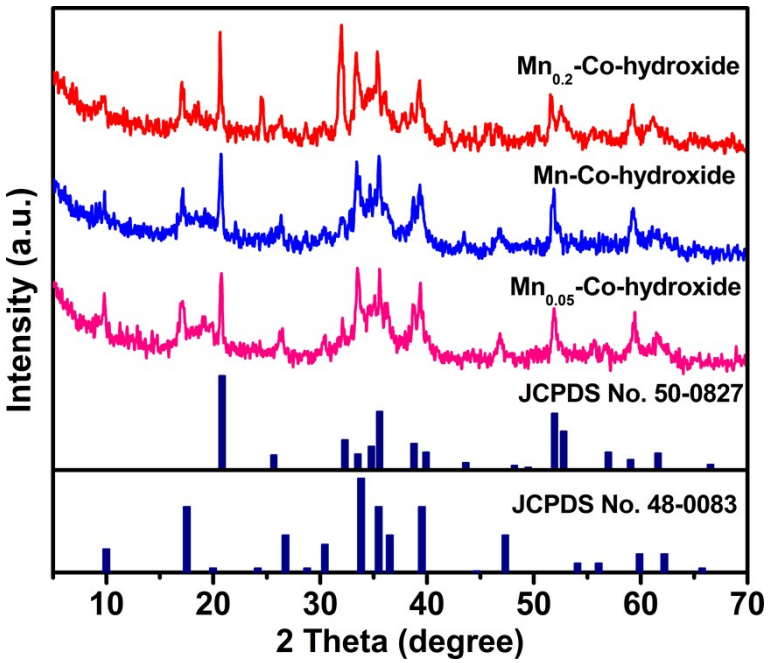

Fig. S1. XRD patterns for $Mn_{0.05}$-Co-hydroxide, Mn-Co-hydroxide and $Mn_{0.2}$-Co-hydroxide precursor.

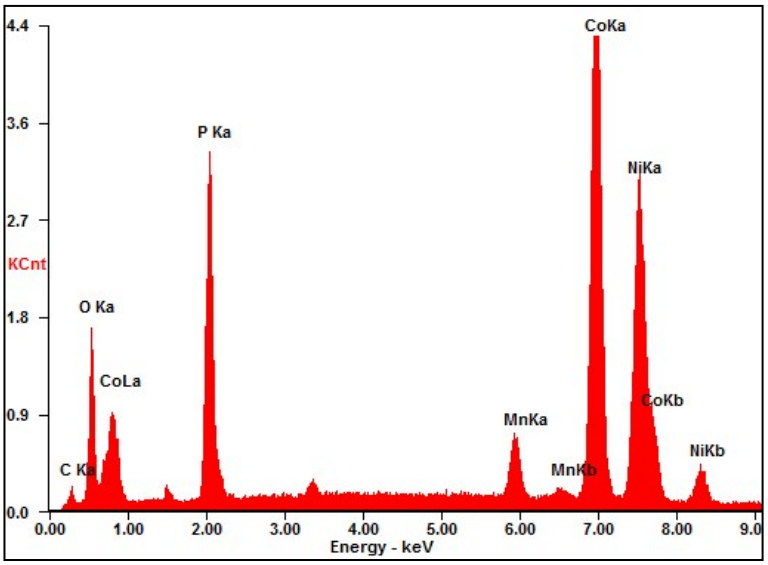

Fig. S2. EDX spectrum for Mn-CoP/NF.

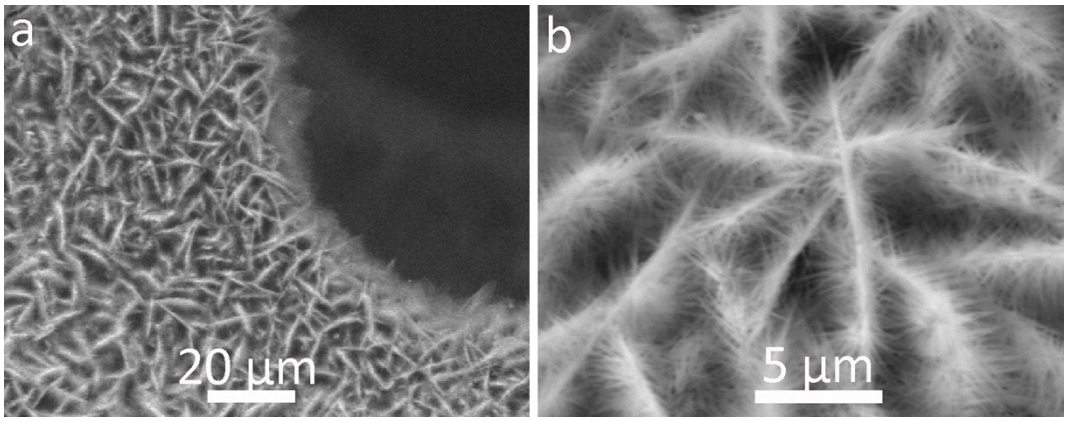

Fig. S3. SEM images for Mn-Co-hydroxide nanoarray precursor.

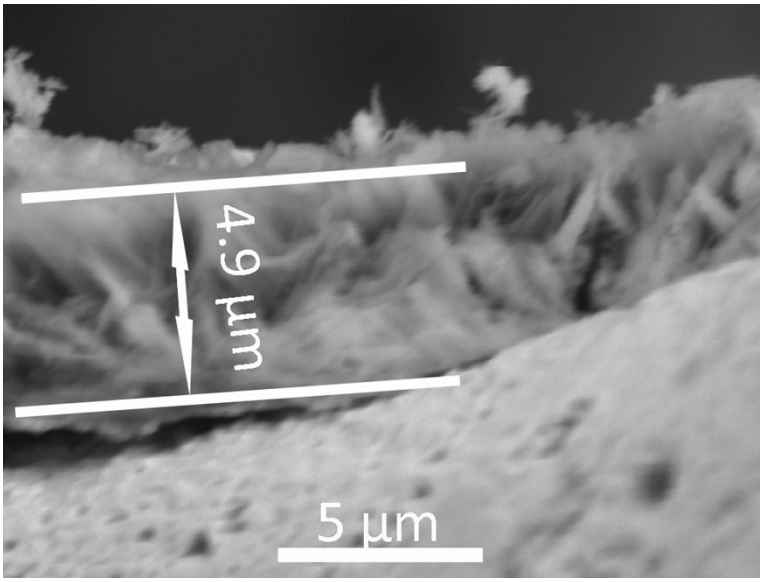

Fig. S4. Cross-section SEM image of Mn-CoP/NF.

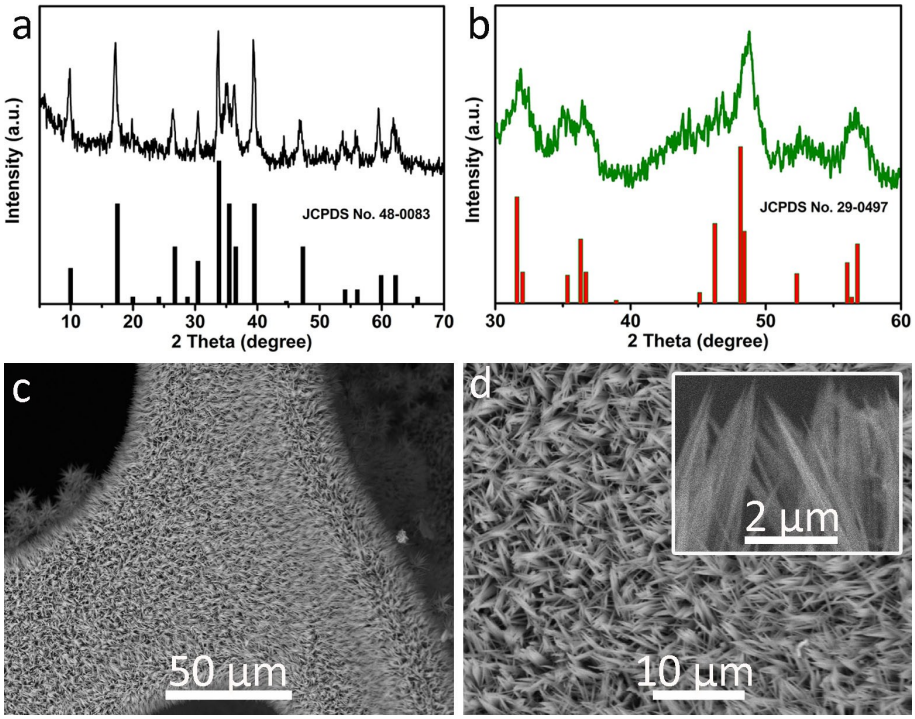

Fig. S5. XRD pattern for (a) CCH and (b) CoP. (c,d) SEM images for CoP/NF.

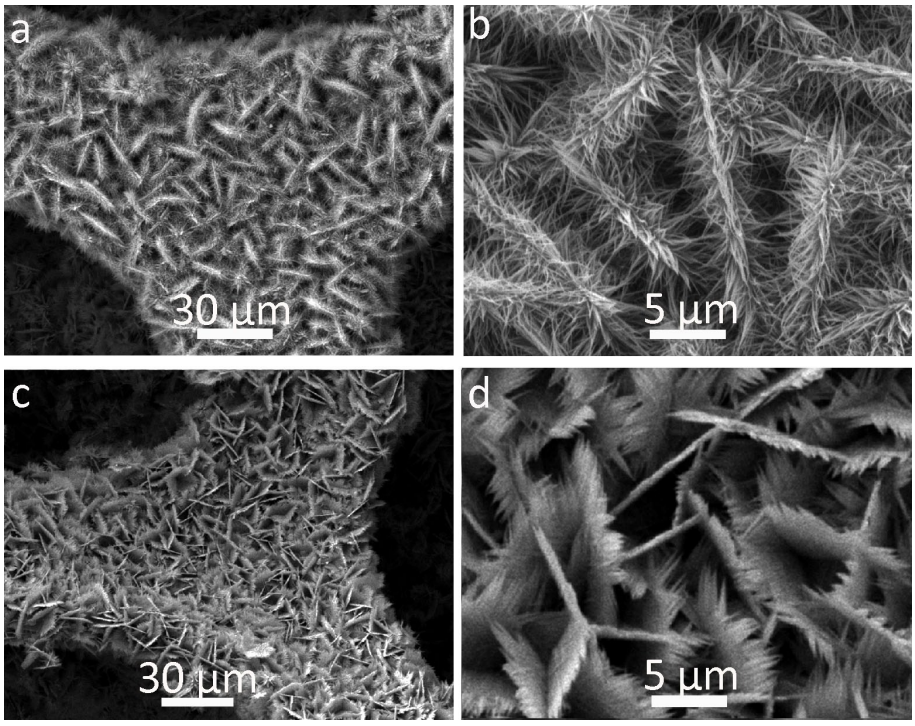

Fig. S6. SEM images for (a,b) $Mn_{0.05}$-CoP/NF and (c,d) $Mn_{0.2}$-CoP/NF.

Table S1. ICP-MS data for $Mn_{0.05}$-CoP, Mn-CoP, and $Mn_{0.2}$-CoP samples.

Catalyst	Mn (ppm)	Co (ppm)	Mn/Co atomic ratio
$Mn_{0.05}$-CoP	1.12	23.35	0.048:1
Mn-CoP	2.48	24.93	0.099:1
$Mn_{0.2}$-CoP	5.06	25.72	0.197:1

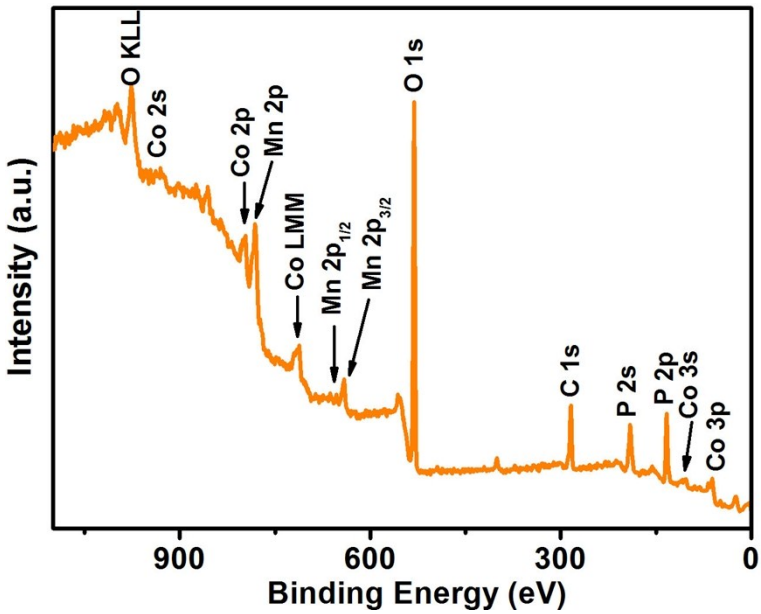

Fig. S7. XPS survey spectrum for Mn-CoP.

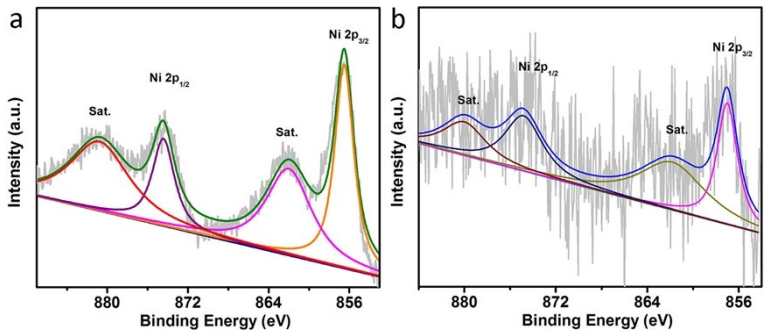

Fig. S8. XPS spectra for (a) bare NF and (b) Mn-CoP/NF in the Ni 2p region.

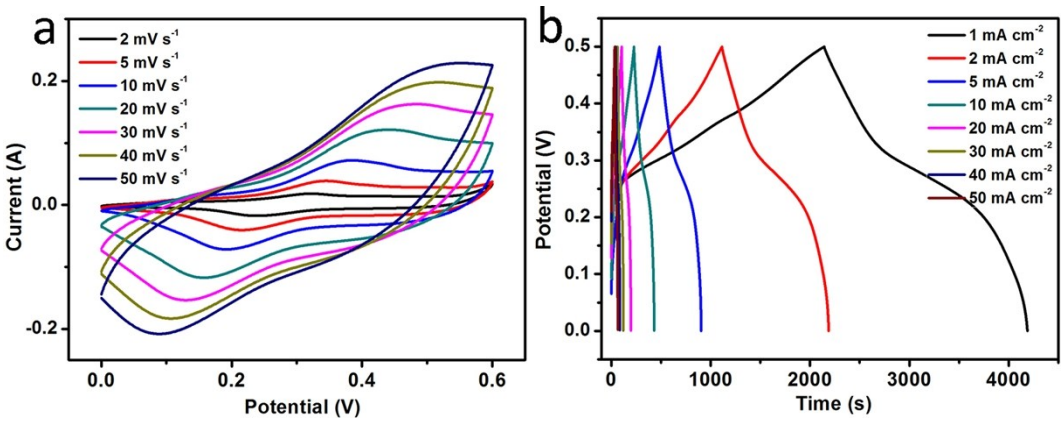

Fig. S9. (a) CV and (b) GCD curves for the CoP/NF electrode.

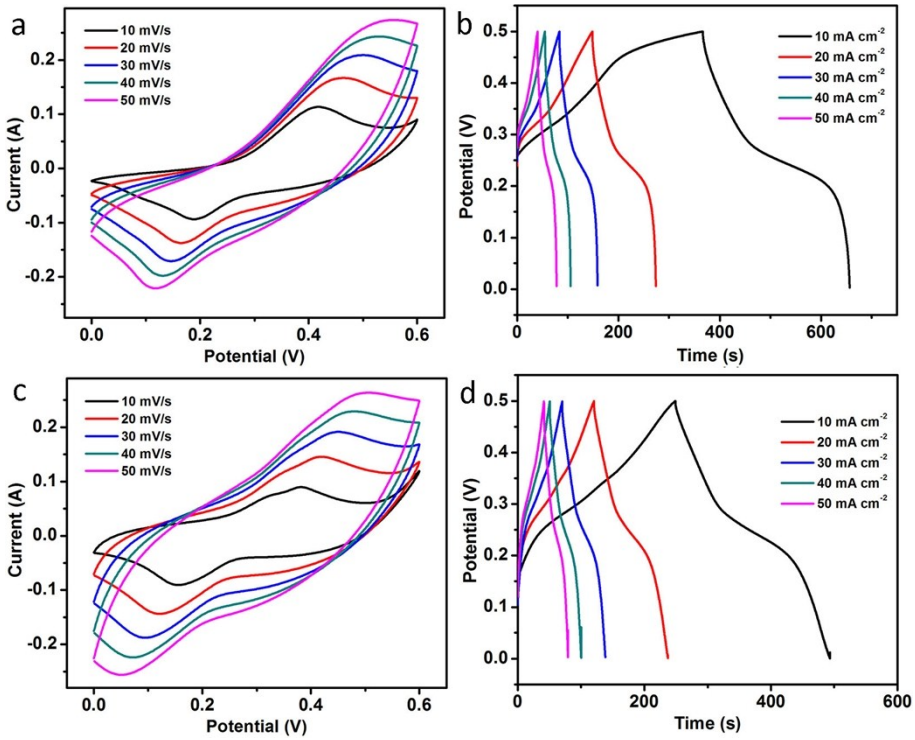

Fig. S10. (a) CV and (b) GCD curves for the $Mn_{0.05}$-CoP/NF electrode. (c) CV and (d) GCD curves for the $Mn_{0.2}$-CoP/NF electrode.

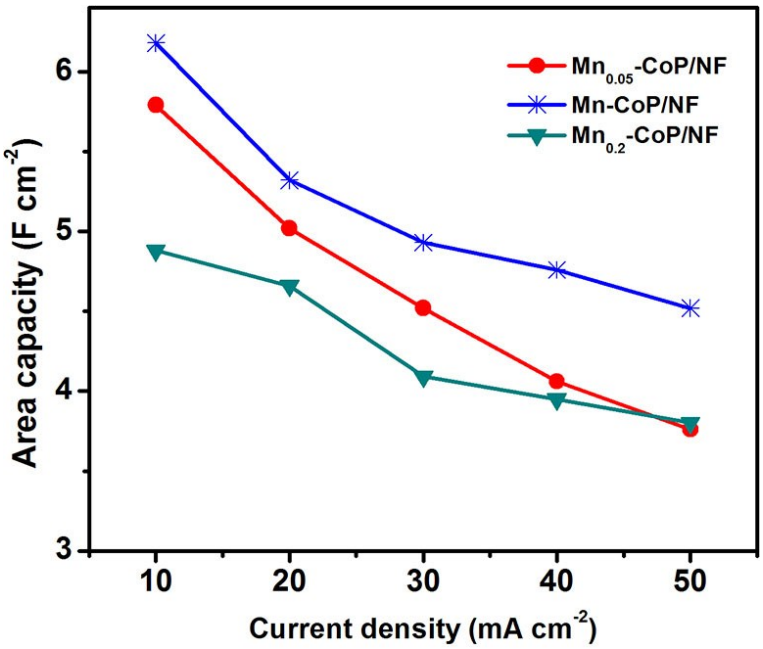

Fig. S11. Dependence of the areal capacitance on current density.

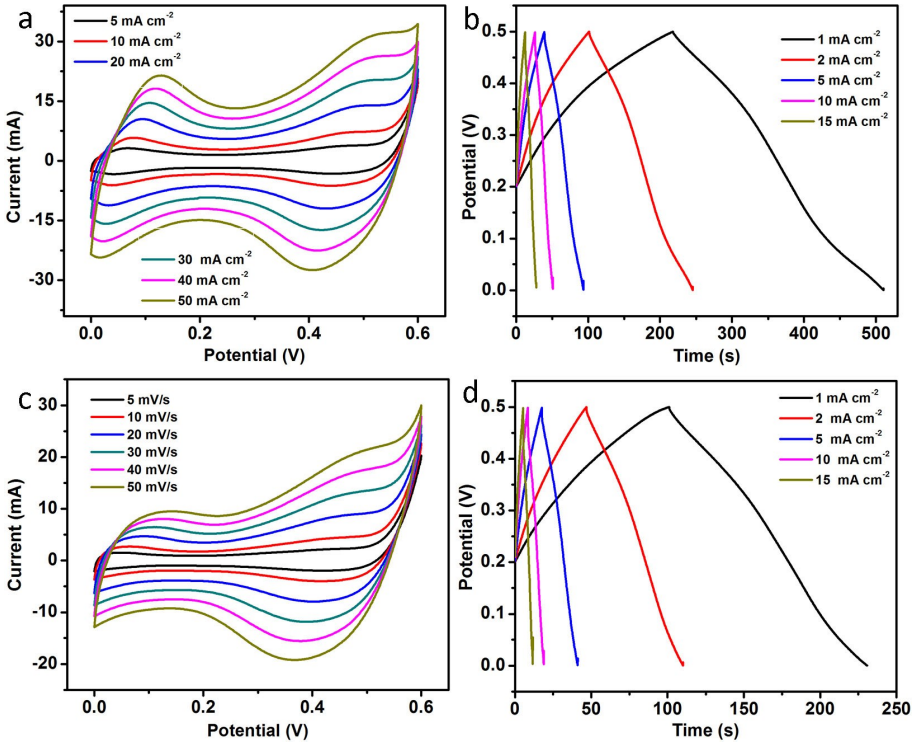

Fig. S12. (a) CV and (b) GCD curves for the Mn-CoP/CC electrode. (c) CV and (d) GCD curves for the Mn-CoP/TM electrode.

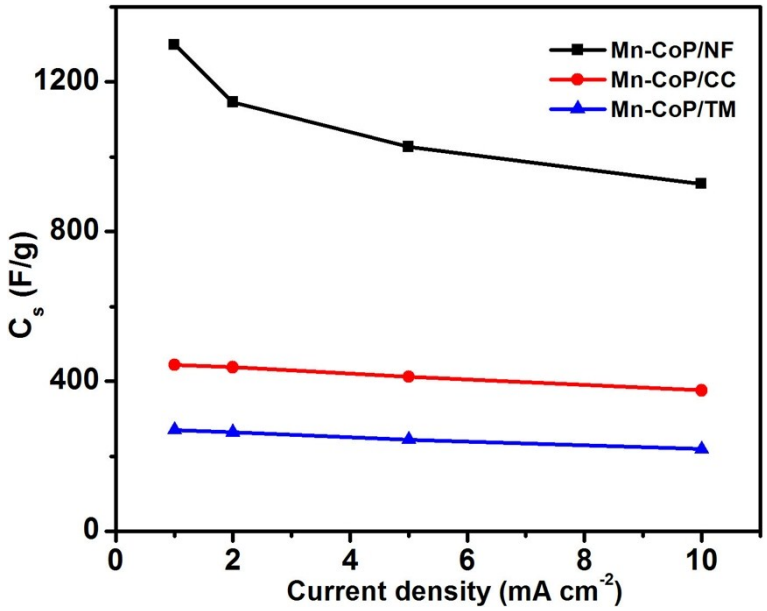

Fig. S13. Dependence of the areal capacitance on current density.

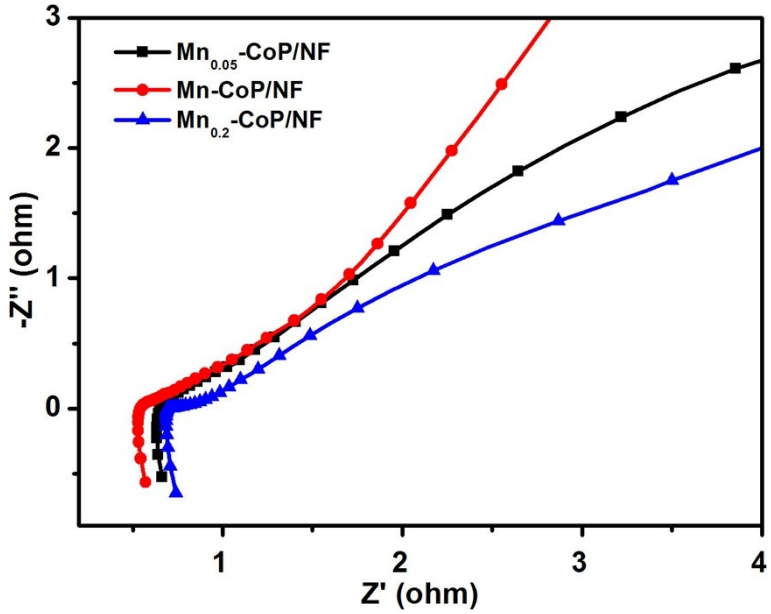

Fig. S14. Nyquist plots for $Mn_{0.05}$-CoP/NF, Mn-CoP/NF, and $Mn_{0.2}$-CoP/NF.

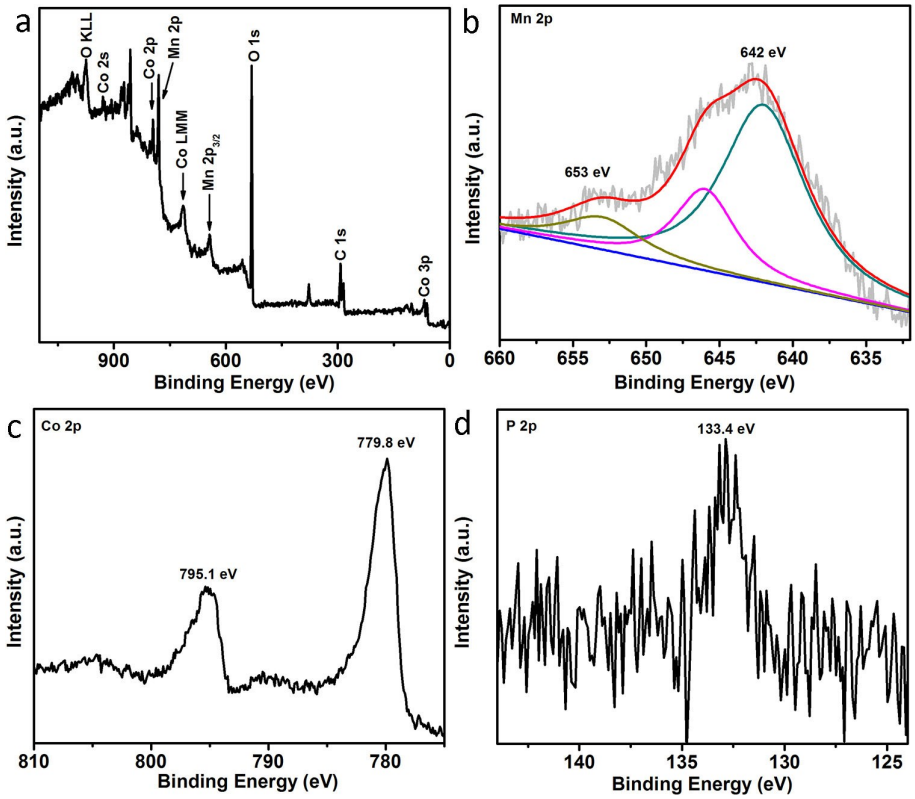

Fig. S15. (a) XPS survey spectrum for Mn-CoP after 2000 cycles between 0 and 0.5 V at 50 mA cm^{-2}. XPS spectra for Mn-CoP after cycling test in the (b) Mn 2p, (c) Co 2p, and (d) P 2p regions.

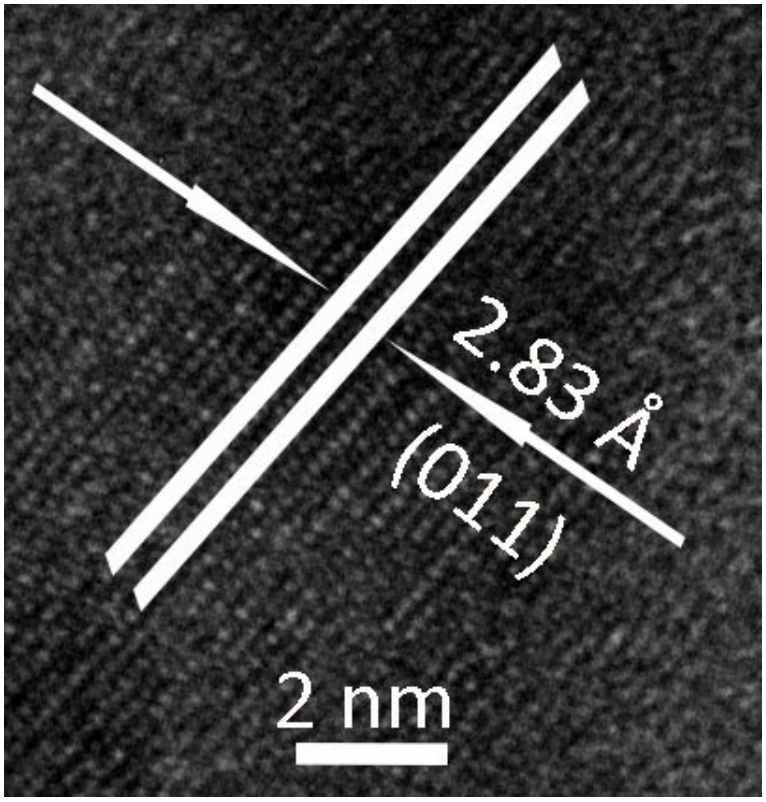

Fig. S16. HRTEM image for Mn-CoP after 2000 cycles between 0 and 0.5 V at 50 mA cm^{-2}.

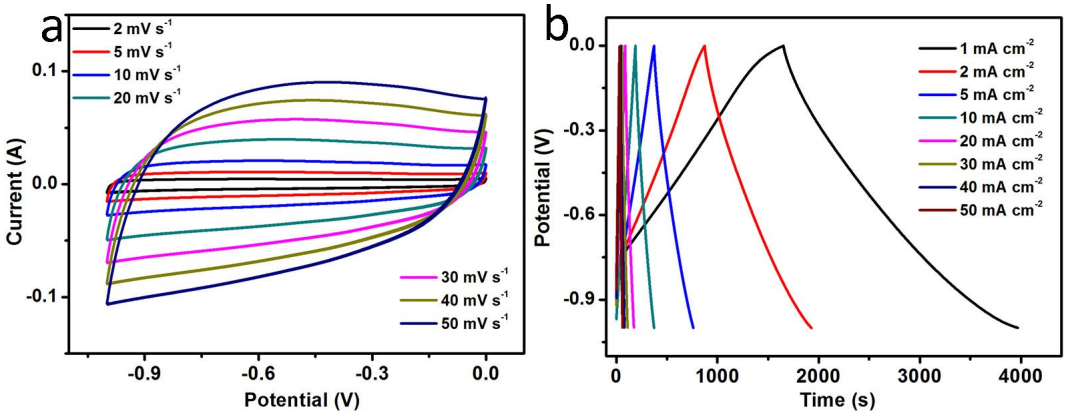

Fig. S17. (a) CV and (b) GCD curves for the AC on NF.

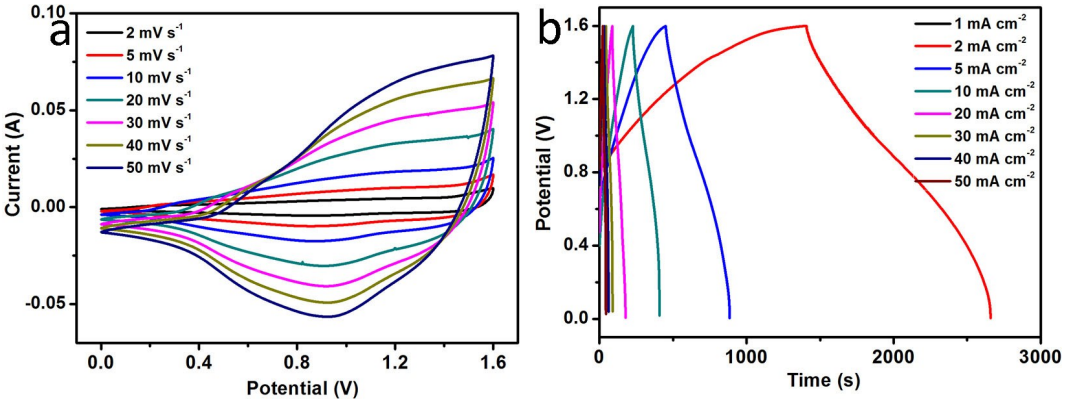

Fig. S18. (a) CV and (b) GCD curves for the CoP//AC device.

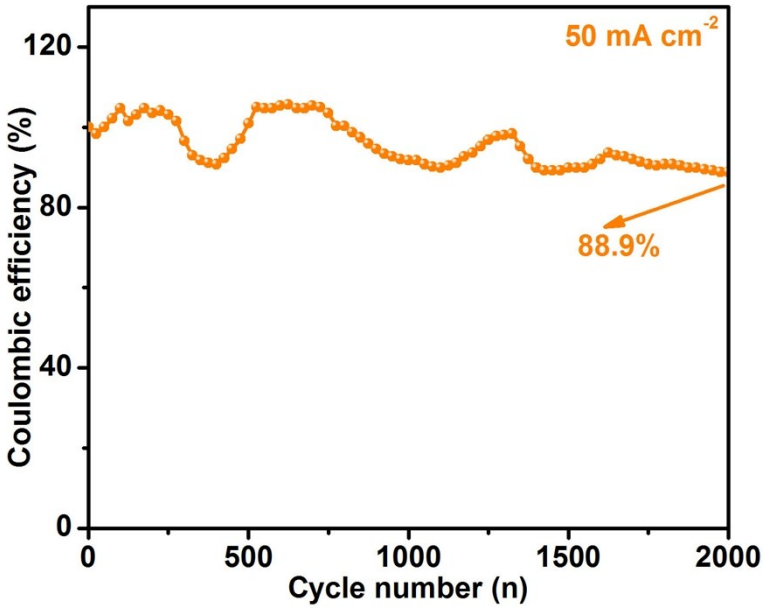

Fig. S19. cycle stability of Mn-CoP//AC device for 4000 cycles at 50 mA cm^{-2}.

Table S2. Comparison of specific capacitances of Mn-CoP/NF with other electrode materials.

Electrode material	Current density (j_s: mA cm^{-2}) (j_m: A g^{-1})	Specific capacitance (C_s: F cm^{-2}) (C_m: F g^{-1})	Ref.
Mn-CoP/NF	j_s: 1 j_m: 0.15	C_s: 8.66 C_m: 1300	This work
	j_s:50 j_m: 7.5	C_s: 4.52 C_m: 679	
CoP/NF	j_s: 1	C_s: 4.47	
	j_s: 50	C_s: 3.11	
Ni_2P-nanosheet/NF	j_s: 3	C_s: 4.1	5
Co_2P nanorods	j_m: 1	C_m: 284	6
Co_2P nanoflowers		C_m: 416	
CoP/CC	j_m: 1	C_m: 342.8	7
Co(P,S)/CC		C_m: 610	
$NiCo_2S_4$@CoS_x nanotube arrays	j_s: 5	C_s: 4.75	8
	j_s: 50	C_s: 2.26	
$NiCo_2O_4$@MnO_2 NW/NF	j_s: 2	C_s: 3.31	9
Ni–Co sulfide NWAs /NF	j_s: 6	C_s: 2.5	10
Ni_3S_2@CoS/NF	j_s: 4	C_s: 4.89	11
$NiCo_2S_4$@PPy-50/NF	j_s: 50	C_s: 3.818	12
Co_3O_4@MnO_2 core/shell nanowire array	j_s: 11.25	C_s: 0.56	13
CoS@$NiCo_2S_4$ NWSAs	j_s: 30	C_s: 7.62	14
$NiCo_2S_4$@CoS_x/NF	j_s: 5	C_s: 4.74	15

MDH-$CoNi_2S_4$ arrays/NF	j_s: 20	C_s: 5.71	16
$CoNi_2S_4$ arrays/NF		C_s: ~3.15	

References

1 L. Mei, T. Yang, C. Xu, M. Zhang, L. Chen, Q. Li and T. Wang, *Nano Energy,* 2014, **3**, 36–45.

2 R. Li, S. Wang, Z. Huang, F. Lu and T. He, *J. Power. Sources*, 2016, **312**, 156–164.

3 H. Chen, J. Jiang, L. Zhang, D. Xia, Y. Zhao, D. Guo, T. Qi and H. Wan, *J. Power. Sources*, 2014, **254**, 249–257.

4 W. Kong, C. Lu, W. Zhang, J. Pu and Z. Wang, *J. Mater. Chem. A*, 2015, **3**, 12452–12460.

5 K. Zhou, W. Zhou, L. Yang, J. Lu, S. Cheng, W. Mai, Z. Tang, L. Li and S. Chen, *Adv. Funct. Mater.*, 2015, **25**, 7530–7538.

6 X. Chen, M. Cheng, D. Chen and R. Wang, *ACS Appl. Mater. Interfaces*, 2016, **8**, 3892–3900.

7 A. M. Elshahawy, C. Guan, X. Li, H. Zhang, Y. Hu, H. Wu, S. J. Pennycook and J. Wang, *Nano Energy*, 2017, **39**, 162–171.

8 W. Fu, C. Zhao, W. Han, Y. Liu, H. Zhao, Y. Ma and E. Xie, *J. Mater. Chem. A*, 2015, **3**, 10492–10497.

9 L. Yu, G. Zhang, C. Yuan and X. W. D. Lou, *Chem. Commun.*, 2013, **49**, 137–139.

10 Y. Li, L. Cao, L. Qiao, M. Zhou, Y. Yang, P. Xiao and Y. Zhang, *J. Mater. Chem. A*, 2014, **2**, 6540–6548.

11 R. Li, S. Wang, J. Wang and Z. Huang, *Phys. Chem. Chem. Phys.*, 2015, **17**, 16434–16442.

12 M. Yan, Y. Yao, J. Wen, L. Long, M. Kong, G. Zhang, X. Liao, G. Yin and Z. Huang, *ACS Appl. Mater. Interfaces*, 2016, **8**, 24525–24535.

13 J. P. Liu, J. Jiang, C. W. Cheng, H. X. Li, J. X. Zhang, H. Gong and H. J. Fan, *Adv. Mater.*, 2011, **23**, 2076.

14 W. Zeng, G. Zhang, X. Wu, K. Zhang, H. Zhang, S. Hou, C. Li, T. Wang and H. Duan, *J. Mater. Chem. A*, 2015, **3**, 24033–24040.

15 W. Fu, C. Zhao, W. Han, Y. Liu, H. Zhao, Y. Ma and E. Xie, *J. Mater. Chem. A*, 2015, **3**, 10492-10497.

16 L. Mei, T. Yang, C. Xu, M. Zhang, L. Chen, Q. Lin, T. Wang, *Nano Energy*, 2014, **3**, 36–45.